Quark number scaling of p_T spectra for Ω and ϕ in relativistic heavy-ion collisions

Jun Song,[1] Feng-lan Shao,[2,*] and Zuo-tang Liang[3,†]

[1]*Department of Physics, Jining University, Shandong 273155, China*

[2]*School of Physics and Engineering, Qufu Normal University, Shandong 273165, China*

[3]*Institute of Frontier and Interdisciplinary Science and Particle Irradiation (MOE), Shandong University, Qingdao, Shandong 266237, China*

(Received 6 March 2020; accepted 13 July 2020; published 30 July 2020)

We show that the experimental data of transverse momentum (p_T) spectra of Ω baryon and ϕ meson at midrapidity in heavy-ion collisions exhibit the constituent quark number scaling in a wide energy range from the Relativistic Heavy Ion Collider to the Large Hadron Collider. Such a scaling behavior is a direct consequence of quark combination mechanism via equal velocity combination and provides a very convenient way to extract the p_T spectrum of strange quarks at hadronization. We present the results of strange quarks obtained from the available data and study the properties in particular the energy dependence of the averaged transverse momentum $\langle p_T \rangle$ and the transverse radial flow velocity $\langle \beta \rangle$ with a hydrodynamics-motivated blast-wave model.

DOI: 10.1103/PhysRevC.102.014911

I. INTRODUCTION

Precision measurements on transverse-momentum (p_T) spectra of hadrons produced in high-energy pp, pA, and AA collisions at the Relativistic Heavy Ion Collider (RHIC) and the Large Hadron Collider (LHC) in the intermediate-p_T region provide us a good opportunity to study the hadronization mechanism and in particular an efficient probe to the created quark matter system—the quark gluon plasma (QGP). We have in particular data for hadrons such as $\Omega^-(sss)$ hyperon and $\phi(s\bar{s})$ [1–9] that consist of only strange quarks and/or antiquarks and are important probe to strangeness-related dynamics of QGP in AA collisions [10–15]. Because they are expected to have relatively small hadronic interaction cross sections [10,11], they suffer from small distortion in the hadronic rescattering stage and therefore carry important information of QGP at hadronization.

In a recent work [16], we showed that the experimental data of p_T spectra of hadrons at midrapidity in high-multiplicity events of p-Pb collisions at LHC energies exhibit a perfect constituent quark number scaling (QNS). Such a scaling behavior is a direct consequence of quark combination mechanism via equal velocity combination (EVC) and might be regarded as a clear signature for creation of QGP. Recently, QNS for hadronic p_T spectra is also valid in high-multiplicity pp collisions at $\sqrt{s} = 7$ and 13 TeV [17,18]. It is natural to ask whether it is also valid in AA collisions.

The study in AA collisions is in principle straightforward. However, since in the intermediate p_T region, for long-lived hadrons, such as pions, kaons, and protons, decay contributions are often important and contaminations from these decays and final-state hadronic interactions are difficult to remove. It is therefore very exciting to see that data on Ω and ϕ have been obtained [1–9] at RHIC and LHC in a very wide energy range from $\sqrt{s_{NN}} = 11.5$ to 2760 GeV.

The p_T spectra of Ω and ϕ provide the best place to test QNS not only because there is little contamination from decay but also due to the fact that in these hadrons only constituent strange quarks and antiquarks are involved so that QNS, if it exists, takes the simplest form. It provides also an ideal place to extract the p_T spectrum for strange quarks.

In this paper, we examine the experimental data of midrapidity p_T spectra of Ω and ϕ in heavy-ion collisions [1–9] and show that such a QNS also exists in the broad energy region from the RHIC and LHC. We extract the strange quark p_T spectrum just before hadronization in relativistic heavy-ion collisions and study the related properties within a hydrodynamics-motivated blast-wave model. These results are given in Secs. II and III. In Sec. IV, we present a short summary and an outlook.

II. THE QNS FOR HADRONIC p_T SPECTRA

QNS was shown to be valid for hadronic p_T spectra in high-multiplicity events in pp and p-Pb collisions at LHC [16,18]. We now examine whether it is also valid in AA collisions by using data on p_T spectra obtained at RHIC and LHC [1–9].

A. QNS for Ω^- and ϕ in AA collisions

We recall that QNS for hadronic p_T spectra in pp and p-Pb collisions at LHC in the intermediate p_T region refers to the number of constituent quarks and is formulated in the following way. For p_T spectra $f_h(p_T) \equiv dN_h/dp_T$ of hadrons consisting of quarks and/or antiquarks of the same flavor, we have

$$f_h(p_T) = \kappa_h f_q^{n_q}(p_T/n_q), \tag{1}$$

*shaofl@mail.sdu.edu.cn

†liang@sdu.edu.cn

 ©2020 American Physical Society

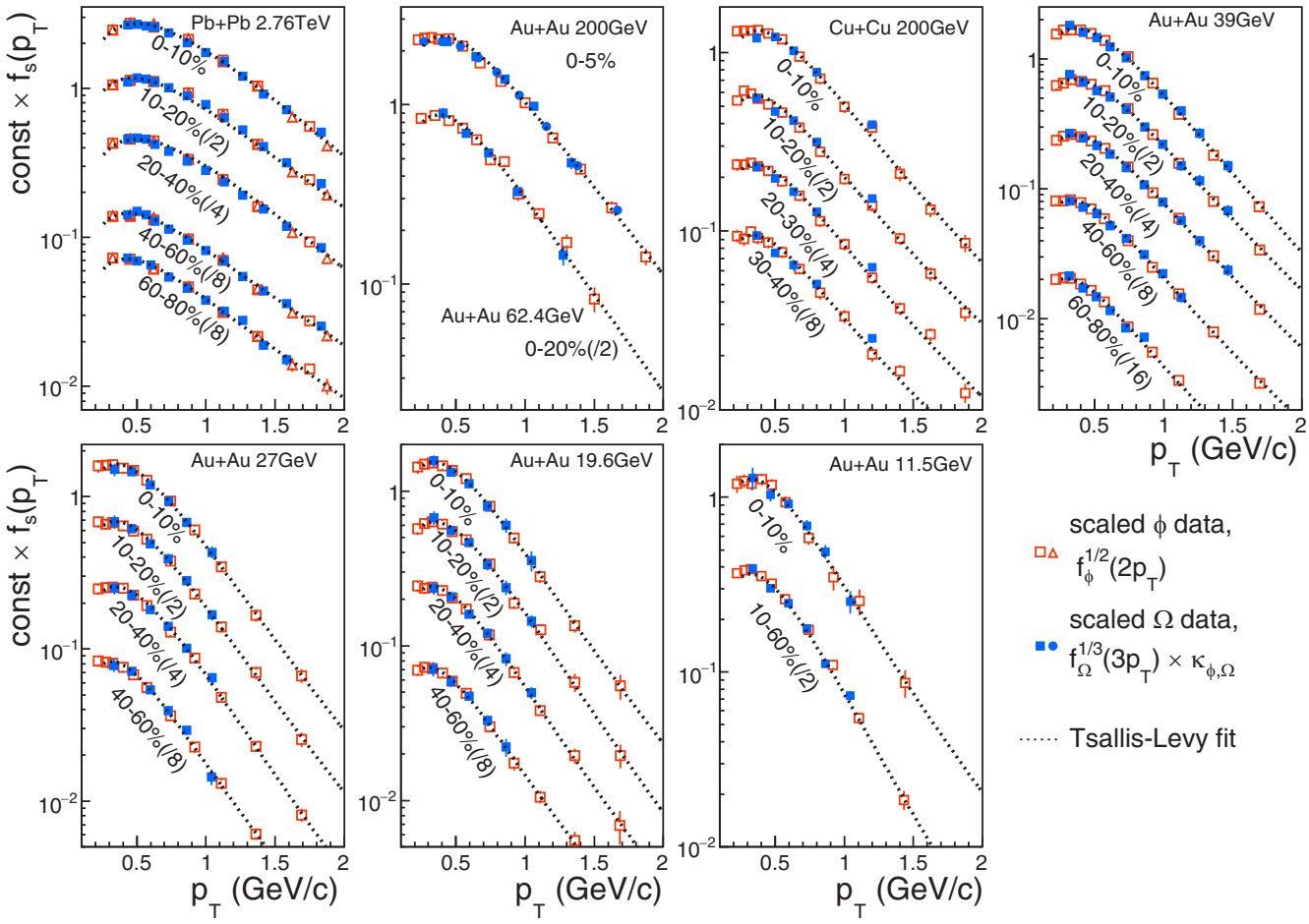

FIG. 1. Test of QNS of p_T spectra of Ω ($\Omega^- + \bar{\Omega}^+$) and ϕ in AA collisions. The constant $\kappa_{\phi,\Omega}$ is adjusted in the way that the results for $\kappa_{\phi,\Omega} f_\Omega^{1/3}(3p_T)$ look to fall in the same lines as those of $f_\phi^{1/2}(2p_T)$. The data are taken from Refs. [1–9]. The dotted lines are simple fittings with the Tsallis-Levy function [22] to guide the eye.

where h denotes hadron, n_q is the number of the constituent quarks and/or antiquarks, and κ_h is a constant independent of p_T but can be different for different hadron h. For a hadron consisting of different flavors of quarks, e.g., for a baryon B consisting of $q_1q_2q_3$, we have

$$f_B(p_T) = \kappa_B f_{q_1}(x_1 p_T) f_{q_2}(x_2 p_T) f_{q_3}(x_3 p_T), \tag{2}$$

where $x_1 + x_2 + x_3 = 1$, $x_1 : x_2 : x_3 = m_{q_1} : m_{q_2} : m_{q_3}$, and m_{q_i} is the constituent quark mass of q_i. The function $f_{q_i}(p_T)$ of p_T is universal for different hadrons and can be identified as the p_T distribution of q_i before hadronization.

It is obvious that for Ω^- and ϕ, QNS takes the simplest form, i.e.,

$$f_{\Omega^-}(3p_T) = \kappa_{\Omega^-} f_s^3(p_T), \tag{3}$$

$$f_\phi(2p_T) = \kappa_\phi f_s(p_T) f_{\bar{s}}(p_T) = \kappa_\phi f_s^2(p_T), \tag{4}$$

and it leads to the equality

$$f_\phi^{1/2}(2p_T) = \kappa_{\phi,\Omega^-} f_{\Omega^-}^{1/3}(3p_T), \tag{5}$$

where the coefficient $\kappa_{\phi,\Omega^-} = \kappa_\phi^{1/2}/\kappa_{\Omega^-}^{1/3}$ is a constant that is independent of p_T but can be dependent on collision energies, centralities, or other parameters. Here we consider the midrapidity region. Since all strange quarks and antiquarks are produced in pairs in the collision process, we take as usual $f_s(p_T) = f_{\bar{s}}(p_T)$, which was used to provide a good description of strange and antistrange hadron p_T spectra at RHIC energies [19–21].

Equation (5) can be used to check whether QNS is valid for the p_T spectra of Ω^- and ϕ in AA collisions. To do this, we take all of the available data on the p_T spectra of Ω ($\Omega^- + \bar{\Omega}^+$) and ϕ in Au + Au collisions at RHIC and in Pb + Pb collisions at LHC [1–9]. We build up $f_\phi^{1/2}(2p_T)$ and $f_\Omega^{1/3}(3p_T)$ and plot them in the same figure. The obtained results are given in Fig. 1. The results for Ω's are multiplied by an arbitrary p_T-independent constant that corresponds to $\kappa_{\phi,\Omega}$ in Eq. (5). This constant is adjusted in the way that the results for $\kappa_{\phi,\Omega} f_\Omega^{1/3}(3p_T)$ look to fall in the same lines as those of $f_\phi^{1/2}(2p_T)$. To guide the eye, we also present simple fittings with the Tsallis-Levy function [22] in the figure.

From Fig. 1, we see clearly that the results obtained from the data of Ω and those of ϕ are well coincident with each other at different energies and different centralities. These results clearly show that QNS exists also in heavy-ion

collisions in such a wide energy range. Besides the normalization constant, the curve in Fig. 1 just corresponds to $f_s(p_T)$, the p_T spectrum of strange quarks before hadronization.

B. QNS and quark combination via EVC

It has been shown that QNS for hadronic p_T spectra is a direct consequence of the quark combination via EVC. The reason is in fact very simple. If we demand that, e.g., a baryon B consisting of $q_1q_2q_3$ is produced through combination of the three constituent quarks with the same velocity β, we obtain immediately from $p_i = \gamma\beta m_i$ that $p_1 : p_2 : p_3 = m_1 : m_2 : m_3$ and the results given by Eqs. (2)–(4). The basic idea of EVC in the quark combination mechanism can be traced back to Ref. [23] and, recently inspired by QNS, has been applied to describe hadronic p_T spectra in different situations [17,18,24,25]. It is also in this mechanism that the universal $f_{q_i}(p_T)$ gets a clear physical significance. It is just the p_T spectrum of q_i before hadronization. In other words, we obtain a simple way to extract the p_T spectra of quarks before hadronization.

The value of the coefficient κ_h depends on the dynamical details in combination such as the baryon-to-meson yield ratio, vector-to-pseudoscalar meson production ratio, strangeness suppression, net quark influence, and so on. It cannot be derived in QNS but should be derived from the hadronization model. In the limiting case where there is no net quark contribution and the numbers of quarks and antiquarks are very large, it has been shown [16] that, in quark combination models, κ_h takes a relatively simple form, i.e.,

$$\kappa_\Omega^{(0)} = \frac{8}{3a} A_{sss}/N_t^2, \tag{6}$$

$$\kappa_\phi^{(0)} = 2\left(1 - \frac{1}{a}\right) A_{ss} C_\phi / N_t, \tag{7}$$

where a superscript (0) is introduced to specify that it is for zero net quark; $N_t = N_q + N_{\bar{q}}$ is the total number of quarks and antiquarks; a is a parameter describing the baryon-to-meson production ratio that was parameterized as [26] $N_M/N_B = 3(a-1)$ in quark combination models; C_ϕ is the conditional probability to produce a ϕ meson from a $s\bar{s}$ under the condition that the $s\bar{s}$ will definitely combine with each other to form a meson. $A_{ss}^{-1} \equiv 2\int dp_T f_s^2(p_T)$ and $A_{sss}^{-1} \equiv 3\int dp_T f_s^3(p_T)$ are determined by integrations of the normalized s quark p_T distribution $f_s(p_T)$ squared and cuboid, respectively.

From Eqs. (6) and (7), we obtain immediately

$$\kappa_{\phi,\Omega}^{(0)} = \frac{3^{1/3}}{\sqrt{2}} \frac{\sqrt{a-1}}{a^{1/6}} \frac{A_{ss}^{1/2}}{A_{sss}^{1/3}} C_\phi^{1/2} N_t^{1/6}. \tag{8}$$

We generalize it to the case of finite quark numbers and nonzero net-quark numbers [16,17] and obtain the following result, up to order of N_t^{-1} and z^2:

$$\kappa_{\phi,\Omega} \approx \kappa_{\phi,\Omega}^{(0)} \left[1 + \frac{2(2+\lambda_s)}{(1-z)\lambda_s N_t} - \frac{1}{18}(a-4)(2a-7)z^2\right], \tag{9}$$

where $\lambda_s \equiv N_{\bar{s}}/N_{\bar{u}}$ is the strangeness suppression factor and $z \equiv (N_q - N_{\bar{q}})/N_t$ is the net-quark fraction in the system. We emphasize in particular that the net quark can only be u or d quark so that it has no influence on the strangeness conservation.

The result given by Eq. (9) is valid generally in the stochastic quark combination models. It depends on the properties of quark composition of the system before hadronization such as the total quark number, the net quark fraction, and the strangeness suppression and also on the hadronization mechanism via baryon-to-meson ratio and the conditional probability C_ϕ. These parameters are empirically known and are extracted from the corresponding data or other empirical facts. The total number of quarks and antiquarks N_t and the net-quark fraction z are determined by the charged hadron multiplicity and antihadron-to-hadron yield ratios (see, e.g., Refs. [19,26,27]). The parameter a is determined as $a = 4.86$ in the light-flavor sector [28]. The strange suppression factor λ_s is determined by yields of strange hadrons kaons and Λ's relative to pions [19,28]. If we take only vector and pseudoscalar meson productions into account, then C_ϕ is determined by the vector-to-pseudoscalar meson production ratio. It can also be determined by the data of the yield ratio ϕ/K^- [2,4,6,9] using the relation $\phi/K^- = \lambda_s C_\phi/(1+\lambda_s C_\phi)$ in the quark combination model. As a test, we show in Fig. 2 values of coefficient $\kappa_{\phi,\Omega}$ (full symbols) obtained in Fig. 1 and those obtained using Eq. (9) (open symbols). The model uncertainties come from those of the parameters, in particular those of C_ϕ and N_t. We see that the agreement with each other is quite satisfactory, which suggests that not only the shapes of p_T spectra but also yields of Ω and ϕ can be described by the combination model under EVC. We also see that there is a very good agreement with a logarithmic fit for the coefficient $\kappa_{\phi,\Omega}$ as a function of $dN_{\rm ch}/d\eta$.

III. THE p_T SPECTRUM OF s QUARKS

As described in Sec. II, QNS provides a convenient way of extracting p_T spectra for quarks before hadronization. Here, from the data on Ω and ϕ [1–9], we obtain the p_T spectrum of strange quarks. It is then interesting to study the related properties based on the extracted results. In this section, we present the results on the energy dependence of the averaged transverse momentum and the radial flow velocity within the blast-wave model [29].

A. The energy dependence of $\langle p_T \rangle$

By fitting the data of Ω and ϕ as given in Fig. 1 in terms of the Tsallis-Levy function [22] of quark p_T distribution, we calculate the averaged transverse momentum $\langle p_T \rangle$ of strange quarks in the soft region $0 < p_T < 2$ GeV/c. The results obtained are shown in Fig. 3 as a function of the charged-particle pseudorapidity density per pair of participant nucleons $(dN_{\rm ch}/d\eta)/(0.5N_{\rm part})$. The error bars are calculated from the uncertainties of the parameters of Tsallis-Levy function in fitting the data with quadratic sums of statistical and

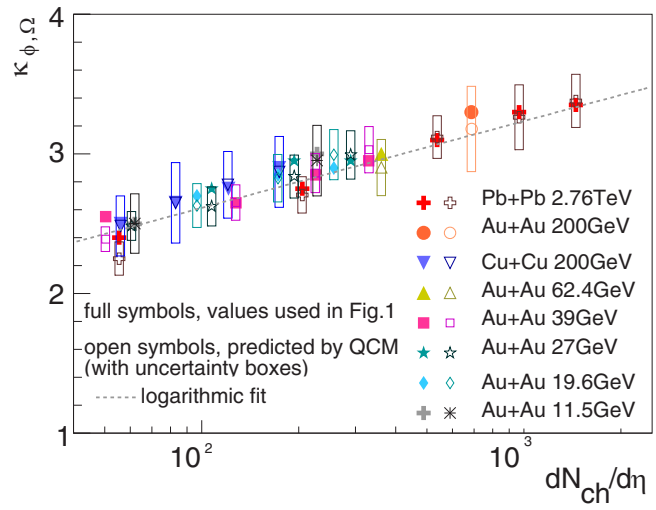

FIG. 2. Coefficient $\kappa_{\phi,\Omega}$ used in Fig. 1, the full symbols, and the predicted values in quark combination model, open symbols with uncertainty boxes.

systematic uncertainties. The dashed line represents a logarithmic fit $\langle p_T\rangle = 0.476 + 0.159\ln[(dN_{\rm ch}/d\eta)/(0.5N_{\rm part})]$ GeV.

From Fig. 3, we see that the transverse momentum $\langle p_T\rangle$ for s quarks before hadronization depends approximately logarithmically on $(dN_{\rm ch}/d\eta)/(0.5N_{\rm part})$. The energy dependence is not significant. We note that in particular those results at $\sqrt{s_{NN}} = 19.6$ and 11.5 GeV are mixed up each other due to the similar $(dN_{\rm ch}/d\eta)/(0.5N_{\rm part})$. The averaged transverse momentum of strange quarks under local thermal equilibrium [29] is about 0.45–0.5 GeV/c at the hadronization temperature ($T \approx 160$ MeV). The obtained $\langle p_T\rangle$ of strange quarks in Fig. 3 is significantly larger than this value. This might suggest a large collective transverse radial flow of strange quarks created in prior parton phase evolution.

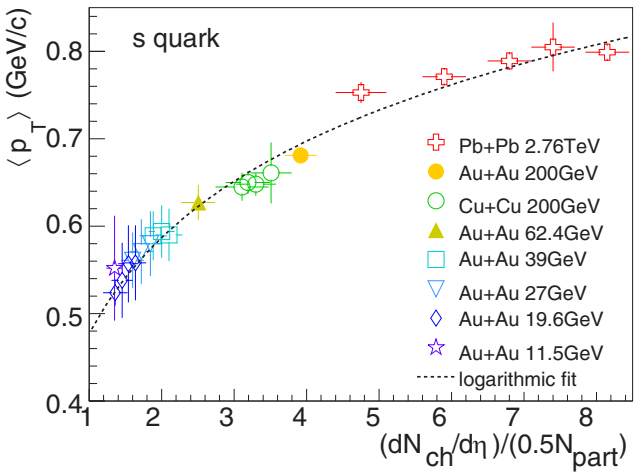

FIG. 3. The average transverse momentum $\langle p_T\rangle$ of strange quarks at midrapidity in heavy-ion collisions. The dashed line is a logarithmic fit.

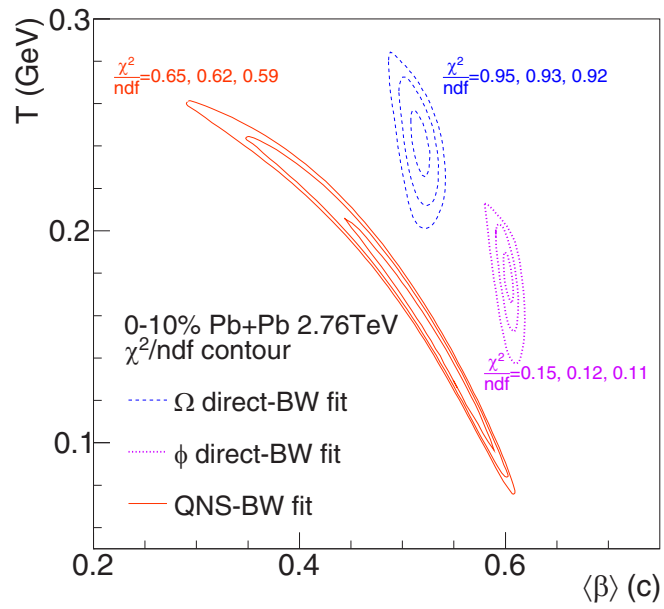

FIG. 4. Contour plot of blast-wave model fit of data of the p_T spectra of Ω and ϕ in central (0–10%) Pb + Pb collisions at $\sqrt{s_{NN}} =$ 2.76 TeV [3,4].

B. The radial flow velocity of strange quarks within the blast-wave model

Using the p_T spectrum obtained in Sec. III A, we can further analyze the radial flow of strange quarks within the hydrodynamics motivated blast-wave model [29]. Here, in this model, it is envisaged that particles are locally thermalized and moving with a collective transverse radial flow velocity field. The p_T distribution is obtained from the superposition of boosted thermal sources at temperature T, i.e., Ref. [29],

$$\frac{dN}{p_T dp_T} \propto \int_0^1 \xi d\xi\, m_T I_0\left(\frac{p_T \sinh\rho}{T}\right) K_1\left(\frac{m_T\cosh\rho}{T}\right), \tag{10}$$

where $\rho = \tanh^{-1}\beta(\xi)$ is the boost angle, I_0 and K_1 are modified Bessel functions, and $m_T = \sqrt{m^2 + p_T^2}$ is the transverse mass. The flow velocity profile is taken as $\beta(\xi) = \beta_s\xi^n$ where ξ is the relative radial position, the form of the profile is controlled by the exponent n, and β_s is the surface velocity. To be compatible with hydrodynamics simulations, we set n to $n \leqslant 2$. We take the temperature T, the averaged flow velocity $\langle\beta\rangle = 2\beta_s/(n+2)$, and the exponent n as fit parameters.

We take the data on p_T spectra of Ω and ϕ in central (0–10%) Pb + Pb collisions at $\sqrt{s_{NN}} = 2.76$ TeV [3,4] as an example and show the fit results of blast-wave model in the ($\langle\beta\rangle$-T) plane in Fig. 4. For comparison, we first make the direct fit at the hadron level for Ω ($p_T \leqslant 6$ GeV/c) and ϕ ($p_T \leqslant 4$ GeV/c), respectively, and then make the fit for the strange quark distribution $f_s(p_T)$ obtained in Fig. 1. The results obtained are marked as direct-BW or QNS-BW fit in the figure.

From Fig. 4, we see that the center region of the direct-BW fit to Ω is far away from that to ϕ. Compared with those

for ϕ mesons, the freeze-out temperature of Ω obtained this way is higher and the velocity is smaller. This would imply that Ω might freeze-out earlier than ϕ in central Pb + Pb collisions at $\sqrt{s_{NN}} = 2.76$ TeV. However, if we do similar fits for data in central Au + Au collisions at $\sqrt{s_{NN}} = 200$ or 39 GeV [1,2,5,6], then we arrive at different conclusions in different cases: At $\sqrt{s_{NN}} = 200$ GeV, the center region of the fit to Ω is lower in temperature and higher in $\langle\beta\rangle$ (which is consistent with the previous report of STAR collaboration [30]), while at 39 GeV, it is lower in temperature and lower in $\langle\beta\rangle$. In other collision energies, the relative position between Ω and ϕ is also variant. This indicates that one could have difficulty to obtain a consistent set of freeze-out parameters for Ω and ϕ by individual blast-wave model fits. In this case, one can only rely on the combined fit for both of them to obtain a common parameter space describing the available data within the accuracy achieved yet.

On the other hand, as inspired by QNS, it could be also interesting to attribute the production of Ω and ϕ to a common source of strange quarks and antiquarks at hadronization and apply the blast-wave model to quark level. From Fig. 4, we see that a characteristic feature of the parameter space of strange quarks is a narrow band across relatively large $\langle\beta\rangle$ or T range in the plane. This is because, in contrast to Ω and ϕ, strange quark has a small mass that has small influence on the shape of the distribution given by Eq. (10). The p_T spectrum of strange quarks is not very sensitive to T itself but determined by $\langle\beta\rangle$ and T in a complementary manner. To determine the $\langle\beta\rangle$ or T, one needs to invoke inputs from studies on other aspects of the quark system. Compared to the direct fits to Ω and/or ϕ, the parameter space of strange quarks has a shift toward a smaller $\langle\beta\rangle$ direction. We observe the same behavior by fitting the data [1,2,5–7,9] at other collision energies.

Such a shift is the consequence of quark combination and can be demonstrated by a simple example. Suppose quark distribution in the rest frame has a Boltzmann form $dN_s/(p_T dp_T) = f_s(p_T)/p_T \propto \exp(-\sqrt{p_T^2 + m_s^2}/T)$ in two-dimensional transverse space; we obtain $f_\phi(p_T)/p_T \propto p_T \exp(-\sqrt{p_T^2 + m_\phi^2}/T)$ and $f_\Omega(p_T)/p_T \propto p_T^2 \exp(-\sqrt{p_T^2 + m_\Omega^2}/T)$ by applying Eqs. (3) and (4) and using $m_\phi \approx 2m_s$ and $m_\Omega \approx 3m_s$. We see that $f_\phi(p_T)$ and $f_\Omega(p_T)$ in the rest frame are broader than Boltzmann distribution by an extra p_T and p_T^2, respectively. This extra p_T dependence will cause larger temperature and/or flow velocity in above direct BW fit for Ω and ϕ.

To see the qualitative behavior of $\langle\beta\rangle$ for strange quarks at hadronization, we simply take $T = T_0(1 - c_2\mu_B^2/T_0^2)$, where μ_B is baryon number chemical potential and is taken as [33] $\mu_B = 1.3075/(1 + 0.288\sqrt{s_{NN}})$ GeV, the curvature $c_2 = 0.0145$ is taken from lattice QCD calculations [34], and T_0 is the temperature at vanishing μ_B and is taken as $T_0 = 164 \pm 5$ MeV [3,27,33,35–38]. Figure 5 shows the results obtained in central collisions at different collision energies. For comparison, we show also results for direct fit to the data of π, K, and p [31,32], which characterize the averaged radial flow at kinetic freeze-out. We see that $\langle\beta\rangle$ of strange quarks increases monotonically with increasing energy. Compared with those for π, K, and proton, the difference seems to be smaller at the LHC energy, implying smaller contributions from the hadronic stage.

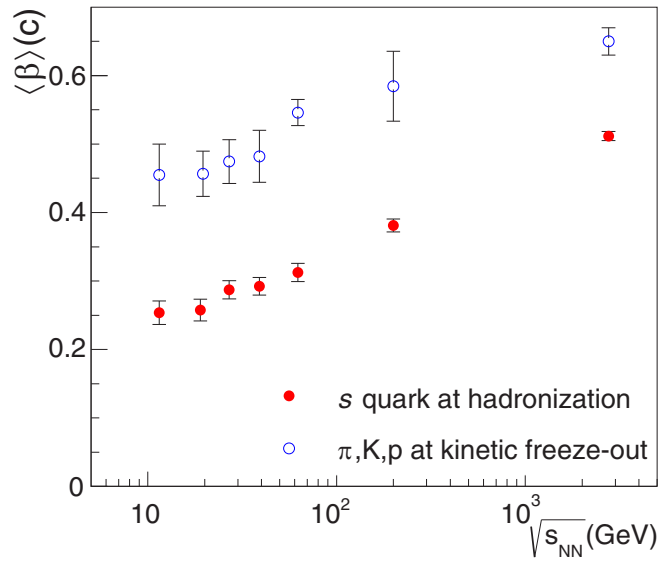

FIG. 5. The averaged radial flow velocity $\langle\beta\rangle$ of strange quarks at hadronization in central heavy-ion collisions extracted from p_T spectrum data of Ω and ϕ at midrapidity compared with those obtained for fitting the π, K, and proton data [31,32].

IV. SUMMARY AND OUTLOOK

To summarize, we show that the experimental data of p_T spectra of Ω and ϕ in AA collisions at both RHIC and LHC energies exhibit also the QNS. This suggests that QNS of p_T spectra found in Refs. [16,18] is not only valid in pA and pp but also in AA collisions and hence is a universal property of p_T spectra of hadrons in all three different kinds of hadronic reactions. The QNS is a direct consequence of quark combination under the rule of EVC. It provides a convenient way of extracting the p_T distribution of quarks from the data for those of hadrons. We extracted in this paper the p_T spectrum of strange quarks from the data of Ω and ϕ and studied its properties such as the average p_T and the radial flow velocity of strange quarks within the blast-wave model. We show that this may get deep insights into the properties of QGP and/or mechanisms of hadronic interactions in high energy collisions.

We also mention that QNS might be used as a test of different mechanisms. As mentioned, quark combinations under EVC provide the most direct and natural explanation. In contrast, we have also checked that, with default parameters, event generators where the fragmentation mechanism is adopted such as PYTHIA [39], Herwig [40], a multiphase transport (AMPT) model [41], and HIJING [42] show significant deviations from QNS. Including color reconnection and/or string overlap effects [43,44] does not significantly improve the case. The QNS might also provide important constraints on details of quark combination mechanism. EVC at the constituent quark level provides the most natural explanation while others, such as the Wigner wave function method

in coalescence models [45–49], the parton recombination [50] with recombination functions determined by the valon model [51,52], and AMPT with string melting that adopts a coalescence mechanism via finite combination radius [53], and so on, all seem to slightly deviate from such precise QNS for p_T spectra of the produced hadrons. Further studies along this direction, both experimentally and theoretically, should be worthwhile and encouraging.

We emphasize once more that the purpose of this paper is to study whether QNS discussed in Refs. [16,18] for pp and pA is also valid in AA collisions. For this purpose, Ω and ϕ production are the best examples and it is very fortunate that we have also data available for the productions of these two hadrons. We have shown that QNS is indeed also valid in this case and we have presented a possible explanation of QNS and examples of further applications in connection to properties of QGP. In Refs. [16,18], we have checked that such QNS is valid in pp and pA not only for hadrons composed of strange quarks but also for those composed of u and/or d quarks. It is also very interesting to check whether this is also the case for AA collisions when corresponding data are available.

ACKNOWLEDGMENTS

We thank S. Y. Li and Q. Wang for helpful discussions. We thank X. L. Zhu for providing us the latest data of Ω^- in Au + Au collisions at $\sqrt{s_{NN}} = 200$ GeV. This work was supported in part by the National Natural Science Foundation of China under Grants No. 11975011, No. 11675092, and No. 11890713, Project of Shandong Province Higher Educational Science and Technology Program (Grant No. J18KA228), and Shandong Province Natural Science Foundation Grants No. ZR2019YQ06 and No. ZR2019MA053.

[1] J. Adams *et al.* (STAR Collaboration), Scaling Properties of Hyperon Production in Au + Au Collisions at $\sqrt{s_{NN}} = 200$ GeV, Phys. Rev. Lett. **98**, 062301 (2007).

[2] B. I. Abelev *et al.* (STAR Collaboration), Measurements of ϕ meson production in relativistic heavy-ion collisions at RHIC, Phys. Rev. C **79**, 064903 (2009).

[3] B. B. Abelev *et al.* (ALICE Collaboration), Multi-strange baryon production at mid-rapidity in Pb-Pb collisions at $\sqrt{s_{NN}} = 2.76$ TeV, Phys. Lett. B **728**, 216 (2014) [Erratum: **734**, 409 (2014)].

[4] B. B. Abelev *et al.* (ALICE Collaboration), $K^*(892)^0$ and $\phi(1020)$ production in Pb-Pb collisions at $\sqrt{s_{NN}} = 2.76$ TeV, Phys. Rev. C **91**, 024609 (2015).

[5] X. Zhu (STAR Collaboration), Ω production in $p + p$, Au + Au and U + U collisions at STAR, in *Proceedings of the 24th International Conference on Ultra-Relativistic Nucleus-Nucleus Collisions (Quark Matter'14)*, Nucl. Phys. A **931**, 1098 (2014).

[6] L. Adamczyk *et al.* (STAR Collaboration), Probing parton dynamics of QCD matter with Ω and ϕ production, Phys. Rev. C **93**, 021903 (2016).

[7] M. M. Aggarwal *et al.* (STAR Collaboration), Strange and multi-strange particle production in Au + Au collisions at $\sqrt{s_{NN}}$ = 62.4 GeV, Phys. Rev. C **83**, 024901 (2011).

[8] G. Agakishiev *et al.* (STAR Collaboration), Strangeness Enhancement in Cu + Cu and Au + Au Collisions at $\sqrt{s_{NN}} =$ 200 GeV, Phys. Rev. Lett. **108**, 072301 (2012).

[9] B. I. Abelev *et al.* (STAR Collaboration), Energy and system size dependence of phi meson production in Cu + Cu and Au + Au collisions, Phys. Lett. B **673**, 183 (2009).

[10] A. Shor, ϕ Meson Production as a Probe of the Quark Gluon Plasma, Phys. Rev. Lett. **54**, 1122 (1985).

[11] H. van Hecke, H. Sorge, and N. Xu, Evidence of Early Multistrange Hadron Freezeout in High-Energy Nuclear Collisions, Phys. Rev. Lett. **81**, 5764 (1998).

[12] C. P. Singh, Comment on "ϕ Meson Production as a Probe of the Quark-Gluon Plasma," Phys. Rev. Lett. **56**, 1750 (1986).

[13] S. A. Bass, A. Dumitru, M. Bleicher, L. Bravina, E. Zabrodin, H. Stöcker, and W. Greiner, Hadronic freezeout following a first-order hadronization phase transition in ultrarelativistic heavy ion collisions, Phys. Rev. C **60**, 021902(R) (1999).

[14] A. Dumitru, S. A. Bass, M. Bleicher, H. Stoecker, and W. Greiner, Direct emission of multiple strange baryons in ultrarelativistic heavy ion collisions from the phase boundary, Phys. Lett. B **460**, 411 (1999).

[15] J. H. Chen, F. Jin, D. Gangadharan, X. Z. Cai, H. Z. Huang, and Y. G. Ma, Parton distributions at hadronization from bulk dense matter produced at RHIC, Phys. Rev. C **78**, 034907 (2008).

[16] J. Song, X.-r. Gou, F.-l. Shao, and Z.-T. Liang, Quark number scaling of hadronic p_T spectra and constituent quark degree of freedom in p-Pb collisions at $\sqrt{s_{NN}} = 5.02$ TeV, Phys. Lett. B **774**, 516 (2017).

[17] X.-r. Gou, F.-l. Shao, R.-q. Wang, H.-h. Li, and J. Song, New insights into hadron production mechanism from p_T spectra in pp collisions at $\sqrt{s} = 7$ TeV, Phys. Rev. D **96**, 094010 (2017).

[18] J.-W. Zhang, H.-H. Li, F.-L. Shao, and J. Song, Constituent quark number scaling from strange hadron spectra in pp collisions at $\sqrt{s} = 13$ TeV, Chin. Phys. C **44**, 014101 (2020).

[19] C.-e. Shao, J. Song, F.-l. Shao, and Q.-b. Xie, Hadron production by quark combination in central Pb + Pb collisions at $\sqrt{s_{NN}} = 17.3$ GeV, Phys. Rev. C **80**, 014909 (2009).

[20] L.-X. Sun, R.-Q. Wang, J. Song, and F.-L. Shao, Hadronic rapidity spectra in heavy ion collisions at SPS and AGS energies in a quark combination model, Chin. Phys. C **36**, 55 (2012).

[21] R.-q. Wang, F.-l. Shao, J. Song, Q.-b. Xie, and Z.-t. Liang, Hadron yield correlation in combination models in high energy AA collisions, Phys. Rev. C **86**, 054906 (2012).

[22] C. Tsallis, Possible generalization of Boltzmann-Gibbs statistics, J. Stat. Phys. **52**, 479 (1988).

[23] Z.-w. Lin and D. Molnár, Quark coalescence and elliptic flow of charm hadrons, Phys. Rev. C **68**, 044901 (2003).

[24] J. Song, H.-h. Li, and F.-l. Shao, New feature of low p_T charm quark hadronization in pp collisions at $\sqrt{s} = 7$ TeV, Eur. Phys. J. C **78**, 344 (2018).

[25] H.-H. Li, F.-L. Shao, J. Song, and R.-Q. Wang, Production of single-charm hadrons by quark combination mechanism in p-Pb collisions at $\sqrt{s_{NN}} = 5.02$ TeV, Phys. Rev. C **97**, 064915 (2018).

[26] J. Song and F.-l. Shao, Baryon-antibaryon production asymmetry in relativistic heavy ion collisions, Phys. Rev. C **88**, 027901 (2013).

[27] F.-l. Shao, J. Song, and R.-q. Wang, Baryon-strangeness correlation in quark combination models, Phys. Rev. C **92**, 044913 (2015).
[28] F.-l. Shao, G.-j. Wang, R.-q. Wang, H.-h. Li, and J. Song, Yield ratios of identified hadrons in p + p, p + Pb, and Pb + Pb collisions at energies available at the CERN Large Hadron Collider, Phys. Rev. C **95**, 064911 (2017).
[29] E. Schnedermann, J. Sollfrank, and U. W. Heinz, Thermal phenomenology of hadrons from 200-A/GeV S + S collisions, Phys. Rev. C **48**, 2462 (1993).
[30] J. Adams *et al.* (STAR Collaboration), Experimental and theoretical challenges in the search for the quark gluon plasma: The STAR Collaboration's critical assessment of the evidence from RHIC collisions, Nucl. Phys. A **757**, 102 (2005).
[31] B. Abelev *et al.* (ALICE Collaboration), Centrality dependence of π, K, p production in Pb-Pb collisions at $\sqrt{s_{NN}} = 2.76$ TeV, Phys. Rev. C **88**, 044910 (2013).
[32] L. Adamczyk *et al.* (STAR Collaboration), Bulk properties of the medium produced in relativistic heavy-ion collisions from the beam energy scan program, Phys. Rev. C **96**, 044904 (2017).
[33] A. Andronic, P. Braun-Munzinger, K. Redlich, and J. Stachel, Decoding the phase structure of QCD via particle production at high energy, Nature **561**, 321 (2018).
[34] C. Bonati, M. D'Elia, F. Negro, F. Sanfilippo, and K. Zambello, Curvature of the pseudocritical line in QCD: Taylor expansion matches analytic continuation, Phys. Rev. D **98**, 054510 (2018).
[35] J. Cleymans, H. Oeschler, K. Redlich, and S. Wheaton, Comparison of chemical freeze-out criteria in heavy-ion collisions, Phys. Rev. C **73**, 034905 (2006).
[36] R. Bellwied, S. Borsanyi, Z. Fodor, S. D. Katz, and C. Ratti, Is There a Flavor Hierarchy in the Deconfinement Transition of QCD? Phys. Rev. Lett. **111**, 202302 (2013).
[37] S. Chatterjee, R. M. Godbole, and S. Gupta, Strange freezeout, Phys. Lett. B **727**, 554 (2013).
[38] M. Bleicher, J. Steinheimer, and R. Stock, The QCD phase diagram from statistical model analysis, in *Walter Greiner Memorial Volume*, edited by P. O. Hess and H. Stöcker (World Scientific Publishing, Singapore, 2018), pp. 41–64.
[39] T. Sjöstrand, S. Ask, J. R. Christiansen, R. Corke, N. Desai, P. Ilten, S. Mrenna, S. Prestel, C. O. Rasmussen, and P. Z. Skands, An introduction to PYTHIA 8.2, Comput. Phys. Commun. **191**, 159 (2015).
[40] M. Bahr *et al.*, Herwig++ physics and manual, Eur. Phys. J. C **58**, 639 (2008).
[41] Z.-W. Lin, C. M. Ko, B.-A. Li, B. Zhang, and S. Pal, A multiphase transport model for relativistic heavy-ion collisions, Phys. Rev. C **72**, 064901 (2005).
[42] X.-N. Wang and M. Gyulassy, HIJING: A Monte Carlo model for multiple jet production in p p, p A, and A A collisions, Phys. Rev. D **44**, 3501 (1991).
[43] A. Ortiz Velasquez, P. Christiansen, E. Cuautle Flores, I. A. Maldonado Cervantes, and G. Paić, Color Reconnection and Flowlike Patterns in *pp* Collisions, Phys. Rev. Lett. **111**, 042001 (2013).
[44] C. Bierlich, G. Gustafson, L. Lönnblad, and A. Tarasov, Effects of overlapping strings in pp collisions, J. High Energy Phys. 03 (2015) 148.
[45] V. Greco, C. M. Ko, and P. Lévai, Parton Coalescence and Anti-Proton/Pion Anomaly at RHIC, Phys. Rev. Lett. **90**, 202302 (2003).
[46] R. J. Fries, B. Muller, C. Nonaka, and S. A. Bass, Hadron production in heavy-ion collisions: Fragmentation and recombination from a dense parton phase, Phys. Rev. C **68**, 044902 (2003).
[47] L. W. Chen, V. Greco, C. M. Ko, S. H. Lee, and W. Liu, Pentaquark baryon production at the Relativistic Heavy Ion Collider, Phys. Lett. B **601**, 34 (2004).
[48] L.-W. Chen and C. M. Ko, ϕ and ω production from relativistic heavy-ion collisions in a dynamical quark coalescence model, Phys. Rev. C **73**, 044903 (2006).
[49] J. Pu, K.-J. Sun, and L.-W. Chen, Extracting strange quark freeze-out information in Pb + Pb collisions at $\sqrt{s_{NN}} = 2.76$ TeV from ϕ and Ω production, Phys. Rev. C **98**, 064905 (2018).
[50] R. C. Hwa and C. B. Yang, Production of phi and omega at RHIC in the recombination model, arXiv:nucl-th/0406072 (2004).
[51] R. C. Hwa, Clustering and hadronization of quarks: A treatment of the low p(t) problem, Phys. Rev. D **22**, 1593 (1980).
[52] R. C. Hwa and C. B. Yang, Parton distributions in the valon model, Phys. Rev. C **66**, 025204 (2002).
[53] Y. J. Ye, J. H. Chen, Y. G. Ma, S. Zhang, and C. Zhong, Ω and ϕ in Au + Au collisions at $\sqrt{s_{NN}} = 200$ and 11.5 GeV from a multiphase transport model, Chin. Phys. C **41**, 084101 (2017).